Shielding current in copper-plated multifilament coated conductor wound into single pancake coil and exposed to normal magnetic field

Amemiya, Naoyuki; Sogabe, Yusuke; Yamano, Satoshi; Sakamoto, Hisaki

OPEN ACCESS
IOP Publishing
Superconductor Science and Technology
Supercond. Sci. Technol. **32** (2019) 115008 (10pp)
https://doi.org/10.1088/1361-6668/ab3f1c

Shielding current in a copper-plated multifilament coated conductor wound into a single pancake coil and exposed to a normal magnetic field

Naoyuki Amemiya[1], **Yusuke Sogabe**[1], **Satoshi Yamano**[2,3] and **Hisaki Sakamoto**[2]

[1] Department of Electrical Engineering, Graduate School of Engineering, Kyoto University, Kyoto-Daigaku-Katsura, Nishikyo, Kyoto 615-8510, Japan
[2] HTS Engineering Department, Furukawa Electric Co., Ltd, 6 Yawatakaigandori, Ichihara 290-8555, Japan
[3] SuperPower Inc., 450 Duane Ave., Schenectady, NY 12304, United States of America

E-mail: amemiya.naoyuki.6a@kyoto-u.ac.jp

Received 12 June 2019, revised 9 August 2019
Accepted for publication 28 August 2019
Published 3 October 2019

Abstract

A single pancake coil wound with a copper-plated multifilament coated conductor, with four filaments, was put in a cusp magnetic field, and the magnetic field was measured near the coil at 30 K. A similar experiment was performed by using another reference single pancake coil wound with a monofilament coated conductor. Numerical electromagnetic field analyses of these coils were carried out, and the calculated shielding current-induced fields (SCIFs) were compared with the measured ones in both coils. The temporal behaviour of the calculated SCIF in the coil wound with the four-filament coated conductor was also compared with a series of exponential components, in which a coupling time constant extrapolated from short sample experiments was used as the time constant of the primary component. Current distributions in the coated conductors wound into the pancake coils were visualised. In particular, the temporal behaviours of the current distributions in the four-filament coated conductor and their influence on the SCIF were discussed.

Keywords: coated conductor, coupling current, coupling time constant, multifilament, screening current, shielding current, striation

(Some figures may appear in colour only in the online journal)

1. Introduction

The shielding current-induced field (SCIF) generated by the persistent eddy current induced in the wide face of a coated conductor is a serious concern in magnets that must generate precise magnetic fields. The SCIF was studied firstly for NMR magnets [1–5] and, then, for accelerator magnets [6–10] as well as MRI magnets [11, 12]. The SCIF in a magnet can be reduced by using a multifilament coated conductor, in which its superconductor layer is striated, i.e. divided, into filaments [13–29]. They have been studied mostly for ac loss reduction, and various striation processes have been proposed: laser striation [15–24], chemical etching [25], mechanical cutting [26], undercutting substrate [27, 28], and *in situ* patterning [29]. Some of these previous studies were done by tape manufacturers: SuperOx [23], Furukawa & SuperPower [24], Bruker [28], and THEVA [29]. Multifilament coated conductors with insulated filaments are ideal to decouple filaments, and, hence, to reduce SCIF, but they do not allow current sharing between filaments in case of local normal transition. Finite transverse conductance between filaments is preferable from the viewpoint of current sharing, which

Table 1. Specifications of coated conductors used in experiments and numerical electromagnetic field analyses.

	Four-filament coated conductor	Monofilament coated conductor
Length	20 m	20 m
Width	4 mm	4 mm
Thickness of coated conductor	94 μm	93 μm
Thickness of superconductor layer (t_s)	1.7 μm	1.7 μm
Number of superconductor filaments	4	—
Critical current measured before striation in liquid nitrogen at self-field	100 A[a]	82 A[a]
Critical current measured after striation in liquid nitrogen at self-field	103 A[a]	—
J_{c0} in equation (4) [b]	1.166×10^{11} A m^{-2}	9.626×10^{10} A m^{-2}
B_{Km} in equation (4) [b]	1.425 T	1.425 T
Width of resistive strip between superconductor filaments in numerical electromagnetic field analyses	50 μm	50 μm

[a] The critical current measurements were done as routine measurements in the manufacturing process, whose error is up to ~5 A.
[b] These values for 20 m coated conductors with which pancake coils were wound were determined based on the critical currents measured at $B = 0.1 - 0.5$ T using a short sample taken from the same lot as the 20 m monofilament coated conductor. It was assumed that B_{Km} of both 20 m coated conductors was same as that of the short sample. J_{c0} of each 20 m coated conductor was given as $(I_{c,20}/I_{c,ss})J_{c0,ss}$ where $I_{c,20}$, $I_{c,ss}$, and $J_{c0,ss}$ are the critical current of the 20 m coated conductor measured in liquid nitrogen at self-field, that of the short sample, and J_{c0} of the short sample, respectively.

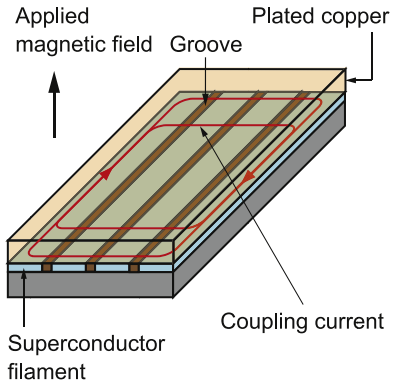

Figure 1. Coupling current flowing through transverse conductance consisting of plated copper. Reproduced from [24]. © IOP Publishing Ltd. CC BY 3.0.

can improve the robustness against local normal transition. However, it should be noted that striations are effective to reduce SCIFs only after the decay of coupling currents, which are the shielding currents flowing through the transverse conductance shown in figure 1 [24]. In this paper, the focus is on a multifilament coated conductor with finite transverse conductance rather than that with insulated superconductor filaments.

Furukawa Electric Co., Ltd and SuperPower Inc. together developed multifilament coated conductors whose superconductor layers were divided into four filaments by laser striation and subsequently were plated with copper using the usual plating process of SuperPower Inc. [24]. In the copper-plated four-filament coated conductor, the plated copper makes current sharing possible between the superconductor filaments. The coupling losses of the stacked short samples were measured to determine their coupling time constants, and it was found that the conductivity of plated copper dominates their transverse conductance [24]. The determined coupling time constants of the stacked short samples were also extrapolated to obtain a scaling law for the coupling time constant against the length of the coated conductor wound into a pancake coil. However, the temporal behaviour of the shielding current in a long copper-plated four-filament coated conductor wound into a pancake coil as well as the SCIF in the coil has not been clarified.

The objective of this study was to clarify the temporal behaviour of the coupling current and the SCIF in a pancake coil wound with the copper-plated four-filament coated conductor. To achieve this objective, a single pancake coil wound with the copper-plated four-filament coated conductor was prepared, as well as a reference single pancake coil wound with a monofilament coated conductor. A magnetic field was applied normal to the coated conductor wound into a coil by putting the coil in a cusp magnetic field. With this configuration, it was possible to study the electromagnetic coupling among filaments in a long multifilament coated conductor wound into a pancake coil by using only one coil. The measured and calculated SCIFs in these two coils were compared, and the temporal behaviour of the calculated coupling current was examined.

This paper is organised as follows. In section 2, the two single pancake coils, each of which was put in a cusp magnetic field, and the experimental setup are described. In section 3, the model for numerical electromagnetic field analyses is given. Section 4 presents results and discussion. Finally, section 5 provides the conclusions.

2. Single pancake coils and experimental setup for applying normal magnetic fields

Two single pancake coils were prepared for the experiments: one wound with a copper-plated four-filament coated conductor, which was striated from one end to the other, and a reference one wound with a monofilament coated conductor. In both coils, the conductor length was 20 m. The specifications of the coated conductors as well as the single pancake coils are listed in tables 1 and 2, respectively. Each coil was put in a cusp magnetic field generated by a pair of double

Table 2. Specifications of single pancake coils used in experiments.

Inner radius	55 mm
Outer radius	61.4 mm
Number of turns	54.2
Separation between turns	25 μm thick polyimide tape co-wound with coated conductor
Face (superconductor layer) of coated conductor	Outside
Impregnation	Paraffin wax

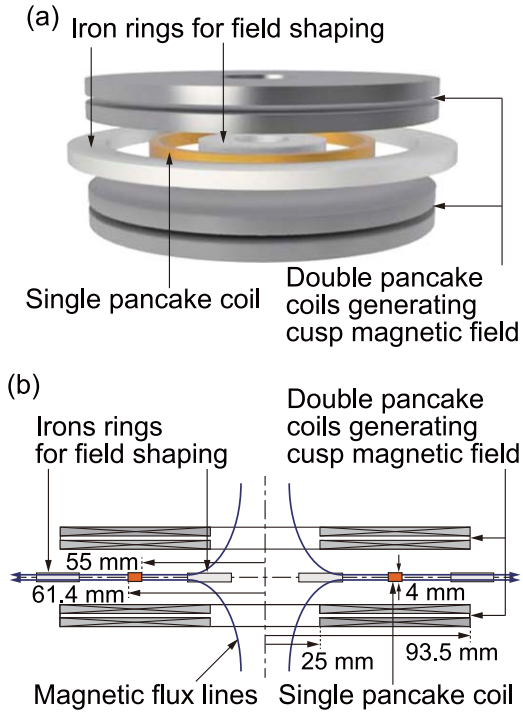

Figure 2. Single pancake coil placed between two double pancake coils, which generate cusp magnetic field, with iron rings for field shaping: (a) perspective view and (b) cross-sectional view.

pancake coils as shown in figures 2(a) and (b). The single pancake coil was placed between two double pancake coils, and the iron rings were placed inside and outside the single pancake coil for field shaping. The single pancake coil was conduction-cooled, but no current was supplied to it. Approximately 0.5 T of normal magnetic field could be applied to the coated conductor of the single pancake coil by providing 43 A of current to the double pancake coils, which were cooled independently of the single pancake coil. With this experimental setup, it was possible to study the electromagnetic behaviour of a long coated conductor wound into a pancake coil in the normal magnetic field rather than a short sample in the normal magnetic field. In other words, it was possible to simulate the electromagnetic condition of a pancake coil in a stack of pancake coils—a top or bottom one, for example—by using only one single pancake coil. It was not possible to study the effect of a multifilament coated conductor by using a single pancake coil to which a transport current is supplied but no external magnetic field is applied. A top view of a single pancake coil is shown in figure 3. A Hall sensor was installed in the coil, with which the radial

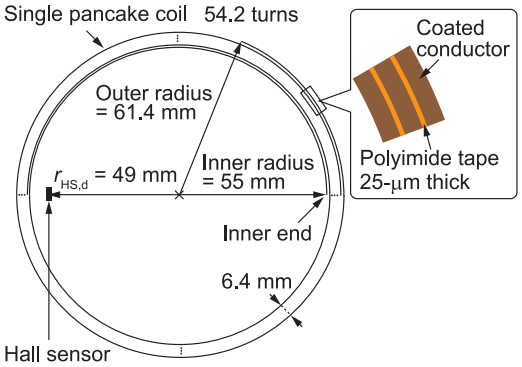

Figure 3. Top view of single pancake coil with Hall sensor, with which one can measure radial component of magnetic field.

component of the magnetic field at $r_{HS} = 49$ mm, where r is the distance from the centre of the single pancake coil, could be measured.

3. Model for electromagnetic field analyses [24, 30]

The current vector potential $\boldsymbol{T}$ defined using current density $\boldsymbol{J}$ as

$$\boldsymbol{J} = \nabla \times \boldsymbol{T} \tag{1}$$

is used for the formulation in the model for electromagnetic field analyses. By using the thin-strip approximation, where only the current density component tangential to the analysed layer is considered [30], the governing equation derived from Faraday's law and Biot–Savart's law is given as follows:

$$\nabla \times \left(\frac{1}{\sigma}\nabla \times \boldsymbol{n}T\right) \cdot \boldsymbol{n} + \frac{\partial}{\partial t}\left(\frac{\mu_0 t_s}{4\pi}\int^{S'} \frac{(\nabla \times \boldsymbol{n}'T') \times \boldsymbol{r} \cdot \boldsymbol{n}}{r^3} \mathrm{d}S'\right) = 0. \tag{2}$$

In this equation, T and T' are the current vector potential components normal to the analysed layer at the field point and source point, respectively; $\boldsymbol{n}$ and $\boldsymbol{n}'$ are the normal vectors of the analysed layer at the field point and source point, respectively; $\boldsymbol{r}$ is the vector from the source point to the field point; t_s is the thickness of the analysed layer; σ is the conductivity of the analysed layer; S' is the entire area of the analysed layer. S' consists of triangular elements and is curved in a coated conductor wound into a coil. The spiral geometry of a single pancake coil was considered, because it was necessary to obtain the coupling current distribution along the coated conductor essentially. The analysed layer consisted of superconducting

filaments, whose width and equivalent conductivity were w_s and σ_s, respectively, and narrow resistive strips between superconductor filaments, whose width and conductivity were w_n and σ_n, respectively [24]. The analyses were made for the upper half of the coil because of its symmetry.

The superconducting property was given by the power law electric field E–current density J characteristic [31, 32]:

$$E = E_0\left(\frac{J}{J_c(B_\perp)}\right)^n, \tag{3}$$

where E_0 is 10^{-4} V m^{-1}, and J_c is the critical current density, which is solely determined by the magnetic field component normal to the superconductor layer $B_\perp$ by Kim's model [33] as

$$J_c(B_\perp) = J_{c0}\frac{B_{Km}}{B_{Km} + |B_\perp|}, \tag{4}$$

where J_{c0} is the critical current density at zero magnetic field, and B_{Km} is a constant. Subsequently, the equivalent conductivity of the superconductor $\sigma_s(\boldsymbol{nT})$ is derived as

$$\sigma_s(\boldsymbol{nT}) = \frac{J}{E} = \frac{J_c(B_\perp)}{E_0}\left(\frac{J_c(B_\perp)}{J}\right)^{n-1} = \frac{J_c(B_\perp)}{E_0} \times \left(\frac{J_c(B_\perp)}{|\nabla \times \boldsymbol{nT}|}\right)^{n-1}. \tag{5}$$

J_{c0} and B_{Km} used for analyses are listed in table 1. To reduce the computation time required for iterative calculations, the maximum equivalent conductivity was set at 10^{30} Ω^{-1} m^{-1}.

The transverse conductance between superconductor filaments G_t, which is the value per unit length along the coated conductor, is represented by narrow resistive strips between superconductor filaments in the model. The conductivity of the resistive strip σ_n is related to the transverse conductance G_t as

$$\sigma_n = \frac{w_n}{t_s}G_t. \tag{6}$$

Algebraic multigrid preconditioning, hierarchical matrices, and parallel computation techniques were used to enhance the performance of computation [34].

4. Results and discussion

4.1. Measured magnetic fields

The single pancake coil wound with the monofilament coated conductor was cooled at 30 and 110 K, the magnetic field was applied, and the radial magnetic field was measured. Figure 4(a) shows the temporal evolutions of the measured magnetic fields $B_m(t)$ as well as the currents supplied to the double pancake coils $I_{dp}(t)$ to generate a magnetic field. Figure 4(b) is the similar plots for the coil wound with the copper-plated four-filament coated conductor. In each figure, $B_m(t)$ at 110 K does not contain the SCIF of the single pancake coil itself, which was not superconducting. In other words, it is the magnetic field generated by the pair of double pancake coils. The double pancake coils were superconducting even when the single pancake coil was at 110 K. Therefore, $B_m(t)$ at 110 K might not be completely proportional to the current supplied to the double pancake coils because of the SCIF of the double pancake coils themselves. The following equation was fit to $B_m(t)$ at 110 K for each coil

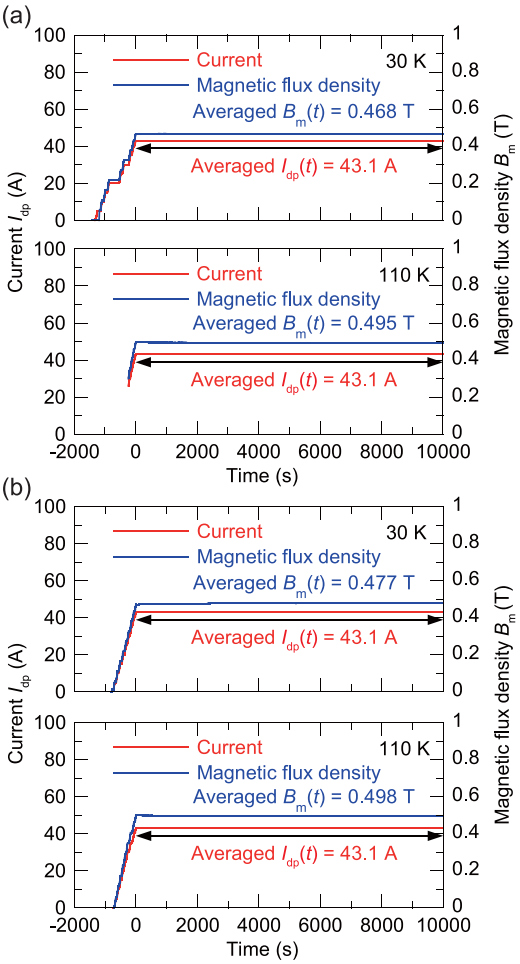

Figure 4. Measured magnetic fields $B_m(t)$ at 110 K, which do not contain SCIF, and those at 30 K, which contain SCIF: (a) single pancake coil wound with monofilament coated conductor and (b) single pancake coil wound with copper-plated four-filament coated conductor.

$$B_{dp,e,ee}(t) = B_{dp0} + B_{dp1}\exp(-t/\tau_{dp1}) + B_{dp2}\exp(-t/\tau_{dp2}), \tag{7}$$

where B_{dp0}, B_{dp1}, B_{dp2}, τ_{dp1}, and τ_{dp2} are fitting parameters. Using fitted values for each coil listed in table 3, $B_{dp,e,ee}$ of equation (7) can be fitted well to $B_m(t)$ at 110 K of each coil. It is assumed that the magnetic field generated by the double pancake coils is reproducible, and, then, $B_{dp,e,ee}(t)$ using parameters listed in table 3 is subtracted from $B_m(t)$ at 30 K to obtain the experimentally-obtained SCIF $B_{sc,e}(t)$ for each coil. The obtained $B_{sc,e}(t)$ of the coil wound with the monofilament coated conductor and that of the coil wound with the copper-plated four-filament coated conductor are compared in figure 5. $B_{sc,e}(t)$ in the coil wound with the four-filament

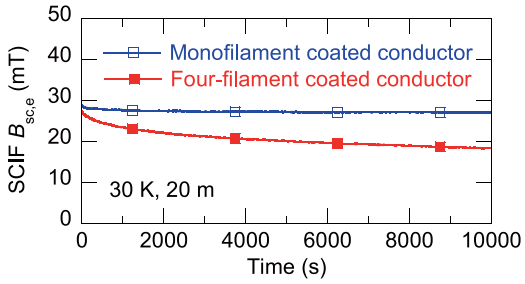

Figure 5. Comparison between experimentally-obtained SCIF $B_{sc,e}(t)$ of single pancake coil wound with monofilament coated conductor and that of single pancake coil wound with copper-plated four-filament coated conductor.

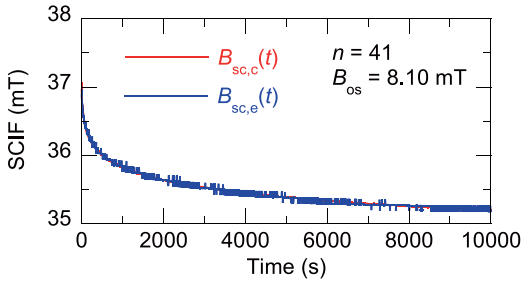

Figure 6. Calculated SCIF $B_{sc,c}(t)$ and experimentally-obtained SCIF $B_{sc,e}(t)$ of single pancake coil wound with monofilament coated conductor when $n = 41$ and $B_{os} = 8.10$ mT.

coated conductor decays much more rapidly than $B_{sc,e}(t)$ in another. Even at the beginning of the flat top of the applied magnetic field ($t = 0$), $B_{sc,e}(t)$ in the coil wound with four-filament coated conductor is smaller than $B_{sc,e}(t)$ in another. The reason for this may be the decay of the coupling current during the field ramp-up.

4.2. Applied magnetic field in electromagnetic field analyses

In the electromagnetic field analyses, it was assumed that the applied magnetic field was uniform. The slight temporal change in the applied magnetic field caused by the decay of SICF of the double pancake coils was also neglected. Then, the applied magnetic field in the electromagnetic field analyses $B_{a,c}(t)$ was given by the following equations:

$$B_{a,c}(t) = B_{a,c,ft}\text{: at flat top,} \tag{8}$$

$$B_{a,c}(t) = \frac{I_{dp}(t)}{I_{dp,ft}} B_{a,c,ft}\text{: during ramp-up,} \tag{9}$$

where $I_{dp}(t)$ in the measurements at 30 K shown in figure 4 was used. $B_{a,c,ft}$ was set at 0.5 T, which was a rounded value of $B_m(t)$ measured at 110 K, and $I_{dp,ft}$ was set at 43.1 A, which was the averaged values at the flat tops in the measurements at 30 K. Using $B_{a,c}(t)$ given by equations (8) and (9), the electromagnetic field analyses were carried out for each coil, and, then, the calculated magnetic fields were subtracted from $B_{a,c}(t)$ to obtain the calculated values of SCIF $B_{sc,c}(t)$.

4.3. Comparison between calculated and measured SCIFs in coil wound with monofilament coated conductor to determine n value

First, the temporal changes of the calculated SCIF $B_{sc,c}(t)$ were compared with the experimentally-obtained SCIF $B_{sc,e}(t)$ in the coil wound with the monofilament coated conductor. The n value of equation (5) and the offset to the measured magnetic field B_{os} were used as fitting parameters. n was varied from 35 to 50. When $n = 41$ and $B_{os} = 8.10$ mT, the temporal change of the calculated SCIF $B_{sc,c}(t)$ agreed well with the measured one $B_{sc,e}(t)$ as shown in figure 6. These n and B_{os} are used in the analyses for all results shown in the latter part of this work. The determined n value reflects E–J characteristic at a low E range, which could indeed govern the temporal behaviour of the shielding current in a long time scale [35]. If the n value had been determined by the usual transport technique, it would have reflected the E–J characteristic at a relatively high E range (around 10^{-4} V m^{-1}) and might have been inappropriate for examining the temporal behaviour of the shielding current in a long time scale.

4.4. Comparison between calculated and measured SCIFs in coil wound with four-filament coated conductor

Next, the temporal changes of the calculated and measured SCIFs in the coil wound with the copper-plated four-filament coated conductor were compared. It was assumed that n of the power law E–J characteristic of the copper-plated four-filament coated conductor is 41 as well. For electromagnetic field analyses, it was necessary to set the conductivity of the narrow resistive strip σ_n, i.e. the transverse conductance between filaments. In previous work, the authors obtained the transverse conductance between filaments $G_{t,ss}$, namely, the conductivity of the resistive strip in the model $\sigma_{n,ss}$, at 77 K from the measurements and calculations of coupling losses of short samples of the copper-plated four-filament coated conductor as follows [24]

$$G_{t,ss}(T = 77\text{ K}) = 3.47 \times 10^7 \Omega^{-1}\,\text{m}^{-1}, \tag{10}$$

$$\sigma_{n,ss}(T = 77\text{ K}) = \frac{w_n}{t_s} G_t = 1.02 \times 10^9 \Omega^{-1}\,\text{m}^{-1}. \tag{11}$$

Here, the subscripts 'ss' mean that the value was obtained from short sample data. This previous work also suggested that the conductivity of plated copper dominates G_t in the copper-plated four-filament coated conductor [24]. If it is assumed that $G_{t,ss}$, namely, $\sigma_{n,ss}$, is determined only by the conductivity of plated copper, $\sigma_{n,ss}$ at temperature T is given as

$$\sigma_{n,ss}(T) = \frac{\sigma_{Cu}(T)}{\sigma_{Cu}(T = 77\text{ K})} \sigma_{n,ss}(T = 77\text{ K}). \tag{12}$$

Table 3. Constants in equation (7), $B_{dp,e,ee}(t) = B_{dp0} + B_{dp1}\exp(-t/\tau_{dp1}) + B_{dp2}\exp(-t/\tau_{dp2})$, with which $B_{dp,e,ee}$ can be fitted well to $B_m(t)$ at 110 K of each coil.

	Four-filament coated conductor		Monofilament coated conductor	
k	B_{dpk}	τ_{dpk}	B_{dpk}	τ_{dpk}
0	0.498 T	—	0.495 T	—
1	0.393×10^{-3} T	2.95×10^{3} s	0.365×10^{-3} T	3.40×10^{3} s
2	0.147×10^{-3} T	155 s	0.141×10^{-3} T	148 s

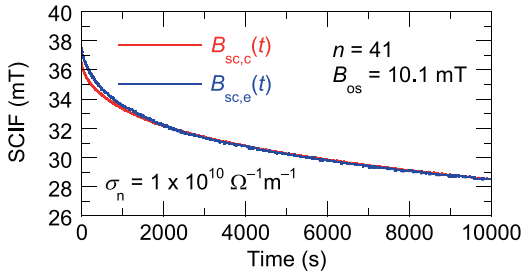

Figure 7. Calculated SCIF $B_{sc,c}(t)$ and experimentally-obtained SCIF $B_{sc,e}(t)$ of single pancake coil wound with copper-plated four-filament coated conductor when $\sigma_n = 1 \times 10^{10}\ \Omega^{-1}\ m^{-1}$, $n = 41$, and $B_{os} = 10.1$ mT.

If it is further assumed that RRR of the plated copper is 45 [36], $\sigma_{Cu}(T = 30\ K)/\sigma_{Cu}(T = 77\ K) = 5.58$ [37], and, then, one obtains

$$\sigma_{n,ss}(T = 30\ K) = 5.69 \times 10^{9}\Omega^{-1}\ m^{-1} \cong 5.7 \times 10^{9}\Omega^{-1}\ m^{-1} \quad (13)$$

We varied σ_n around this value, $5 \times 10^{9}\ \Omega^{-1}m^{-1}$ through $2 \times 10^{10}\ \Omega^{-1}\ m^{-1}$, including $5.7 \times 10^{9}\ \Omega^{-1}\ m^{-1}$, and carried out the electromagnetic field analyses. B_{os} as well as σ_n was used as the fitting parameter when comparing the calculated SCIF $B_{sc,c}(t)$ with the experimentally-obtained SCIF $B_{sc,e}(t)$. When $\sigma_n = 1 \times 10^{10}\ \Omega^{-1}\ m^{-1}$ and $B_{os} = 10.1$ mT, $B_{sc,c}(t)$ can be fitted well to $B_{sc,e}(t)$ except at the beginning of the flat top of the applied magnetic field ($t = 0$–2000 s) as shown in figure 7. These σ_n and B_{os} as well as n of 41 are used in the analyses for all results shown in the latter part of this work.

4.5. Decay time constants of SCIF in coil wound with four-filament coated conductor

In a previous study, it was pointed out that the coupling time constant τ_c corresponding to the entire length l of a coated conductor wound into a pancake coil is given as follows [24]:

$$\tau_1 = al^2. \quad (14)$$

The constant a, which is proportional to the transverse conductance between filaments, was approximately 2 s m^{-2} at 77 K for the copper-plated four-filament coated conductor [24]. Considering $\sigma_{n,ss}(T = 77\ K) = 1.02 \times 10^{9}\ \Omega^{-1}\ m^{-1}$ as shown in equation (11) and $\sigma_n(T = 30\ K) = 1 \times 10^{10}\ \Omega^{-1}\ m^{-1}$, with which $B_{sc,c}(t)$ can be fitted well to $B_{sc,e}(t)$, one can reasonably assume that the constant a might be around 20 s m^{-2} at 30 K:

$$\tau_1 = 20l^2 \text{ at } 30\ K. \quad (15)$$

Table 4. Constants in equation (18), $B_{sc,ee3}(t) = B_0 + B_1\exp(-t/\tau_1) + B_2\exp(-t/\tau_2) + B_3\exp(-t/\tau_3)$, with which $B_{sc,ee3}(t)$ can be fitted well to $B_{sc,c}(t)$ of pancake coil wound with four-filament coated conductor in the entire period between $t = 0$ and 10 000 s.

k	B_k	τ_k
0	26.5 mT	—
1	7.17 mT	8×10^{3} s
2	2.19 mT	693 s
3	0.59 mT	55.4 s

Because the length of the four-filament coated conductor wound into the pancake coil in this work was 20 m, τ_1 becomes 8000 s. First, the following equation was fit to $B_{sc,c}(t)$ in the period between $t = 2000$ and 10 000 s, where $B_{sc,c}(t)$ agrees well with $B_{sc,e}(t)$, using B_0 and B_1 as fitting parameters:

$$B_{sc,ee1}(t) = B_0 + B_1\exp(-t/\tau_1);\ \tau_1 = 8000\ s. \quad (16)$$

Using B_0 and B_1 as listed in table 4, $B_{sc,ee1}(t)$ can be fitted well to $B_{sc,c}(t)$ in the period.

In the earlier period between $t = 0$ and 2000 s, $B_{sc,c}(t)$ contains the following residual, which decays rapidly:

$$B_{sc,c}(t) - B_{sc,ee1}(t). \quad (17)$$

Two exponential components were fit with shorter time constants to this residual. Consequently, a series of exponential components $B_{sc,ee3}(t)$ given as equation (18) can be fitted well to $B_{sc,c}(t)$ in the entire period between $t = 0$ and 10 000 s using B_0 through B_3 and τ_1 through τ_3 as listed in table 4

$$B_{sc,c}(t) \cong B_{sc,ee3}(t) = B_0 + B_1\exp(-t/\tau_1) + B_2\exp(-t/\tau_2) + B_3\exp(-t/\tau_3). \quad (18)$$

$B_{sc,c}(t)$ and $B_{sc,ee3}(t)$ are compared in figure 8. In this figure, each term in equation (18) is also plotted. The first term in equation (18) represents the field induced by persistent shielding current in superconductor filaments, and the second term represents the field induced by the coupling current flowing in the entire length of the coated conductor. The origin of the third and fourth terms with shorter time constants is discussed in the next section.

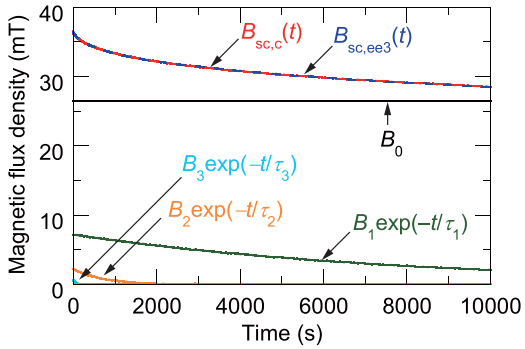

Figure 8. Comparison between calculated SCIF $B_{sc,c}(t)$ of single pancake coil wound with a copper-plated four-filament coated conductor and a series of exponential components: $B_{sc,ee3}(t) = B_0 + B_1\exp(-t/\tau_1) + B_2\exp(-t/\tau_2) + B_3\exp(-t/\tau_3)$ where the constants are listed in table 4.

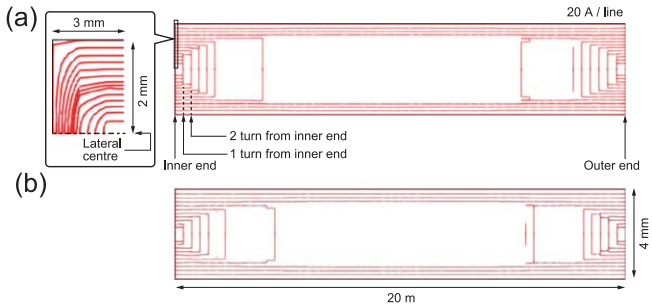

Figure 9. Temporal evolution of current lines in monofilament coated conductor wound into a single pancake coil: (a) $t = 0$ and (b) $t = 10\,000$ s. It should be noted that the figure is expanded laterally for visibility.

4.6. Calculated current distributions in coated conductors and temporal behaviours of SCIF

Figures 9 and 10 show the current lines in the monofilament coated conductor wound into a coil and in the four-filament coated conductor wound into a coil, respectively. It should be noted that the figures are expanded laterally for visibility. The loops of currents in both figures are shielding currents induced by electromagnetic induction during the ramp-up of the cusp magnetic field, which is normal to the wide face of the coated conductor. At $t = 0$ in each figure, one can observe multiple loops of shielding current whose spatial characteristic lengths are different: some expand to the entire length of the coated conductor, and some are localised near the ends of the coated conductor. If a uniform magnetic field is applied to a straight coated conductor that was not wound into a pancake coil, the loops of the shield current could have a single characteristic length, expanding to the entire length of the coated conductor. A coated conductor wound into a pancake coil exposed to a cusp magnetic field is analogous to the stacked short pieces of a coated conductor exposed to a normal magnetic field. Inner or outer turns of the pancake coil behave similarly to coated conductors near the top or the bottom of the stack. If the applied magnetic field is not large enough to penetrate to the lateral centre of the coated

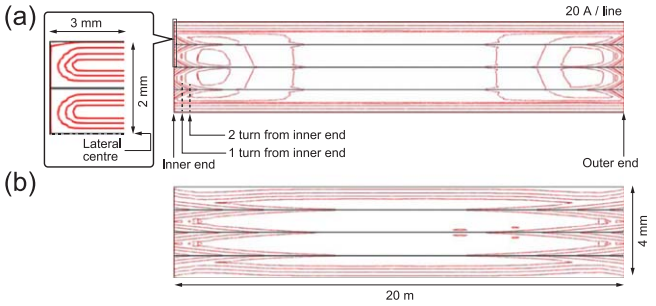

Figure 10. Temporal evolution of current lines in copper-plated four-filament coated conductor wound into a single pancake coil: (a) $t = 0$ and (b) $t = 10\,000$ s. It should be noted that the figure is expanded laterally for visibility.

conductor in the middle of the pancake coil or the stack, more shielding current could be induced in the inner or outer turns of the pancake coil or the coated conductors near the top or the bottom of the stack. This might be the mechanism of the multiple loops of shielding current with different characteristic lengths.

Whereas the loops of current are rather persistent in the monofilament coated conductor as shown in figure 9, the loops of current in the four-filament coated conductor vary temporally as shown in figure 10, because they contain coupling current, which flows through the transverse conductance (resistance) and is not persistent. In particular, coupling current with a short characteristic length decays rapidly, because the inductance is proportional to the length and the transverse resistance is inversely proportional to the length. Such a rapidly decaying coupling current with a short characteristic length could be the origin of the components with short time constants in the SCIF, such as the third and the fourth terms in equation (18).

Next, lateral current distributions across each coated conductor were examined at various longitudinal positions as listed in table 5. Because the magnetic flux penetrates in almost the same way from the inner end and the outer end of a coated conductor wound into a pancake coil, locations between the inner end and the longitudinal centre of a coated conductor were chosen.

Figure 11 shows the lateral current distributions across the monofilament coated conductor at $t = 0$ and 10 000 s. The magnetic flux hardly penetrates to the lateral centre of the coated conductor—in particular, at the longitudinal centre of the coated conductor (position D). Because the shielding current is rather persistent, the temporal changes in the current distributions are not remarkable. A finite E–J characteristic of the superconductor, i.e. a finite nonlinear resistivity of the superconductor, caused slight temporal changes in the current distributions [8, 35], which led to the gradual decay of the SCIF shown in figure 6.

Figure 12 shows the lateral current distributions across the four-filament coated conductor at $t = 0$ and 10 000 s. Near the end of the coated conductor (positions A and B), filaments are decoupled even at $t = 0$. At position C, which is 3.53 m from the inner end of the coated conductor, filaments

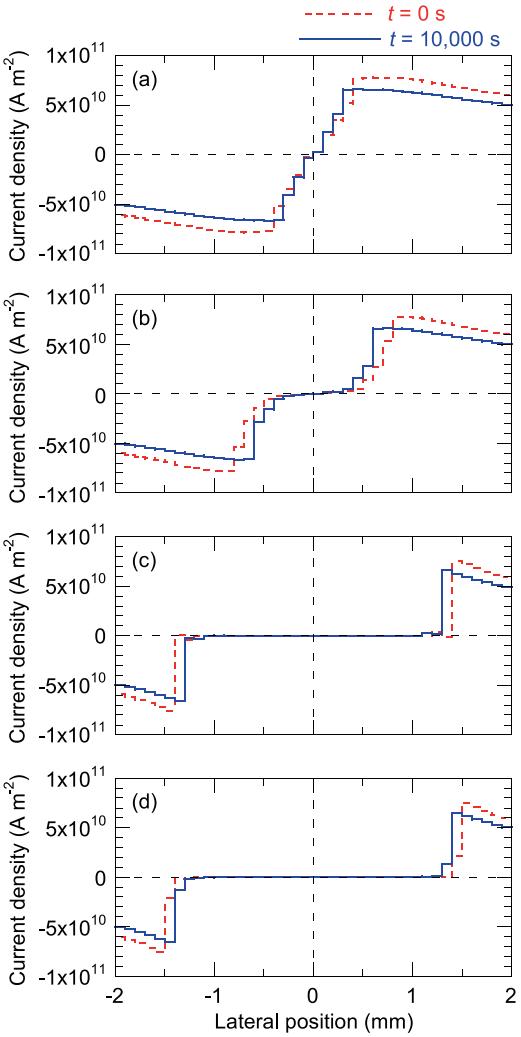

Figure 11. Current distributions across the monofilament coated conductor at various longitudinal positions listed in table 5 at $t = 0$ and 10 000 s: (a) position A, (b) position B, (c) position C, and (d) position D.

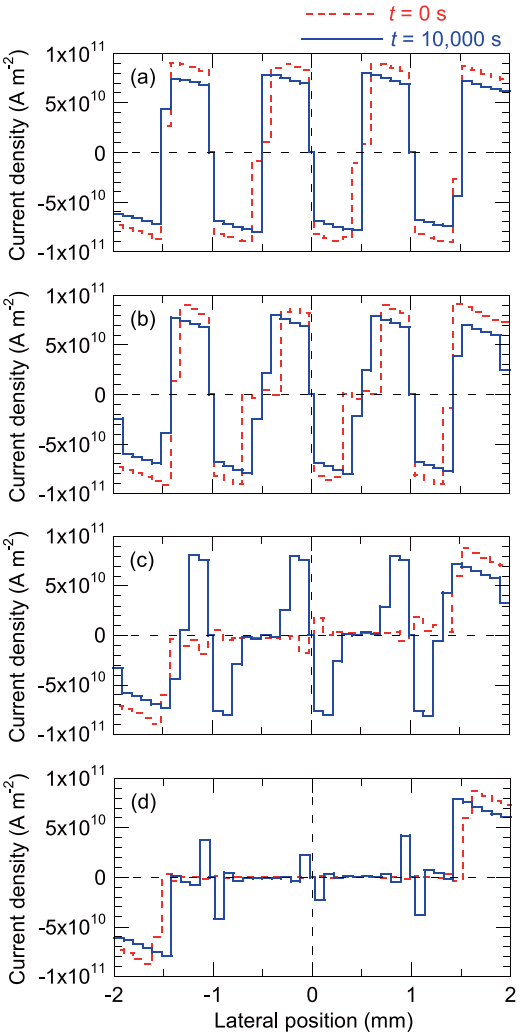

Figure 12. Current distributions across the copper-plated four-filament coated conductor at various longitudinal positions listed in table 5 at $t = 0$ and 10 000 s: (a) position A, (b) position B, (c) position C, and (d) position D.

Table 5. Longitudinal positions in the coated conductor wound into a pancake coil at which lateral current distributions across it are plotted.

Position	Turn from inner end of coated conductor	Distance from inner end of coated conductor
A	0.1 turn	0.034 m
B	1.1 turn	0.380 m
C	10.1 turn	3.53 m
D	27.1 turn	9.65 m

are coupled at $t = 0$ but are decoupled at $t = 10\,000$ s. Such a decoupling process of filaments leads to the rapid decay of the SCIF in the coil wound with the four-filament coated conductor as shown in figure 7. At the longitudinal centre of the coated conductor (position D), which is 9.65 m from the inner end of the coated conductor, filaments are almost coupled even at $t = 10\,000$ s. As discussed in section 4.5, the time constant of the dominant coupling current, which flows in the entire length of the coated conductor, is 8000 s. This is consistent with the coupled filaments at the longitudinal centre of the coated conductor at $t = 10\,000$ s, because a time around the coupling time constant is not long enough to decouple filaments at the longitudinal centre of multifilament coated conductor [24].

5. Conclusion

We measured and calculated the SCIF in a pancake coil wound with a 20 m long copper-plated four-filament coated conductor and in another pancake coil wound with a monofilament coated conductor with the same length, both of which were exposed to 0.5 T of the magnetic field which was normal to their tape faces. The measured and calculated temporal behaviours of the SCIF agreed well with each other: the SCIF decayed more rapidly in the pancake coil wound with the copper-plated four-filament coated conductor than in the pancake coil wound with a monofilament coated

conductor. Electromagnetic field analysis shows that the decay of the SCIF in the pancake coil wound with the copper-plated four-filament coated conductor was dominated by the coupling current flowing in the entire length of the coated conductor and that coupling currents localised near the ends of the coated conductor generated additional minor components with short time constants.

Acknowledgments

This work was supported in part by JSPS KAKENHI Grant Number 16H02326.

ORCID iDs

Naoyuki Amemiya https://orcid.org/0000-0002-3000-864X
Yusuke Sogabe https://orcid.org/0000-0003-1692-629X

References

[1] Hahn S, Bascuñán J, Kim W, Bobrov E, Lee H and Iwasa Y 2008 Field mapping, NMR lineshape, and screening currents induced field analyses for homogeneity improvement in LTS/HTS NMR magnets *IEEE Trans. Appl. Supercond.* **18** 856–9
[2] Amemiya N and Akachi K 2008 Magnetic field generated by shielding current in high T_c superconducting coils for NMR magnets *Supercond. Sci. Technol.* **21** 095001
[3] Uglietti D, Yanagisawa Y, Maeda H and Kiyoshi T 2010 Measurements of magnetic field induced by screening currents in YBCO solenoid coils *Supercond. Sci. Technol.* **23** 115002
[4] Yanagisawa Y, Kominato Y, Nakagome H, Hu R, Takematsu T, Takao T, Uglietti D, Kiyoshi T, Takahashi M and Maeda H 2011 Magnitude of the screening field for YBCO coils *IEEE Trans. Appl. Supercond.* **21** 1640–3
[5] Bang J, Kim S, Jang J Y, Hwang Y J, Cho M, Kim J, Lee J T, Ahn M C, Lee S and Hahn S 2019 Field measurement and analysis of a 3 T 66 mm no-insulation HTS NMR magnet with screening current and manufacturing uncertainty considered *IEEE Trans. Appl. Supercond.* **29** 4601305
[6] Ueda H *et al* 2014 Measurement and simulation of magnetic field generated by screening currents in HTS coil *IEEE Trans. Appl. Supercond.* **24** 4701505
[7] Amemiya N, Otake H, Sano T, Nakamura T, Ogitsu T, Koyanagi K and Kurusu T 2015 Temporal behaviour of multipole components of the magnetic field in a small dipole magnet wound with coated conductors *Supercond. Sci. Technol.* **28** 035003
[8] Amemiya N, Sogabe Y, Sakashita M, Iwata Y, Noda K, Ogitsu T, Ishii Y and Kurusu T 2016 Magnetisation and field quality of a cosine-theta dipole magnet wound with coated conductors for rotating gantry for hadron cancer therapy *Supercond. Sci. Technol.* **29** 024006
[9] Dilasser G, Fazilleau P and Tixador P 2017 Experimental measurement and numerical simulation of the screening current-induced field decay in a small ReBCO coil *IEEE Trans. Appl. Supercond.* **27** 4900204
[10] Fazilleau P, Borgnolutti F, Dilasser G and Durante M 2018 Screening currents within the EuCARD HTS dipole *IEEE Trans. Appl. Supercond.* **28** 4604605
[11] Noguchi S and Cingoski V 2017 Simulation of screening current reduction effect in REBCO coils by external AC magnetic field *IEEE Trans. Appl. Supercond.* **27** 4701405
[12] Miyazaki H *et al* 2017 Screening-current-induced magnetic field of conduction-cooled HTS magnets wound with REBCO-coated conductors *IEEE Trans. Appl. Supercond.* **27** 4701705
[13] Grilli F and Kario A 2016 How filaments can reduce AC losses in HTS coated conductors: a review *Supercond. Sci.Technol.* **29** 083002
[14] Carr W J Jr and Oberly C E 1999 Filamentary YBCO conductors for AC applications *IEEE Trans. Appl. Supercond.* **9** 1475–8
[15] Cobb C B, Barnes P N, Haugan T J, Tolliver J, Lee E, Sumption M, Collings E and Oberly C E 2002 Hysteretic loss reduction in striated YBCO *Physica* C **382** 52–6
[16] Amemiya N, Kasai S, Yoda K, Jiang Z, Levin G A, Barnes P N and Oberly C E 2004 AC loss reduction of YBCO coated conductors by multifilamentary structure *Supercond. Sci. Technol.* **17** 1464–71
[17] Sumption M, Collings E and Barnes P 2005 AC loss in striped (filamentary) YBCO coated conductors leading to designs for high frequencies and field-sweep amplitudes *Supercond. Sci.Technol.* **18** 122–34
[18] Amemiya N, Yoda K, Kasai S, Jiang Z, Levin G A, Barnes P N and Oberly C E 2005 AC loss characteristics of multifilamentary YBCO coated conductors *IEEE Trans. Appl. Supercond.* **15** 1637–42
[19] Majoros M, Glowacki B A, Campbell A M, Levin G A, Barnes P N and Polak M 2005 AC losses in striated YBCO coated conductors *IEEE Trans. Appl. Supercond.* **15** 2819–22
[20] Machi T, Nakao K, Kato T, Hirayama T and Tanabe K 2013 Reliable fabrication process for long-length multi-filamentary coated conductors by a laser scribing method for reduction of AC loss *Supercond. Sci. Technol.* **26** 105016
[21] Demenčík E, Grilli F, Kario A, Nast R, Jung A, Vojenčiak M, Scheiter J and Goldacker W 2015 AC magnetization loss and transverse resistivity of striated YBCO coated conductors *IEEE Trans. Appl. Supercond.* **25** 8201405
[22] Iwakuma M, Nabekura K, Yun K, Yoshida K, Sato S, Tomioka A, Konno M, Ibi A, Machi T and Izumi T 2017 Scribing effect on shielding current in REBCO superconducting coils *IEEE Trans. Appl. Supercond.* **27** 4700806
[23] Godfrin A, Kario A, Gyuráki R, Demenčík E, Nast R, Scheiter J, Mankevich A, Molodyk A, Goldacker W and Grilli F 2017 Influence of the striation process and the thickness of the Cu-stabilization on the AC magnetization loss of striated *RE*BCO tape *IEEE Trans. Appl. Supercond.* **27** 5900809
[24] Amemiya N, Tominaga N, Toyomoto R, Nishimoto T, Sogabe Y, Yamano S and Sakamoto H 2018 Coupling time constants of striated and copper-plated coated conductors and the potential of striation to reduce shielding-current-induced fields in pancake coils *Supercond. Sci. Technol.* **31** 025007
[25] Abraimov D, Gurevich A, Polyanskii A, Cai X Y, Xu A, Pamidi S, Larbalestier D and Thieme C L H 2008 Significant reduction of AC losses in YBCO patterned coated conductors with transposed filaments *Supercond. Sci. Technol.* **21** 082004
[26] Yanagisawa Y, Xu Y, Jin X, Nakagome H and Maeda H 2015 Reduction of screening current-induced magnetic field of REBCO coils by the use of multi-filamentary tapes *IEEE Trans. Appl. Supercond.* **25** 6603705

[27] Fujita S *et al* 2017 Characterization of multifilamentary REBCO coated conductor coil fabricated by using the process of scratching the IBAD-MgO layer *IEEE Trans. Appl. Supercond.* **27** 6600504
[28] Wulff A C *et al* 2015 Two level undercut-profile substrate for filamentary $YBa_2Cu_3O_7$ coated conductors *Supercond. Sci. Technol.* **28** 072001
[29] Kopera L, Šmatko V, Prusseit W, Polák M, Semerad R, Štrbík V and Šouc J 2008 *In situ* patterning of filamentary YBCO coated conductors *Physica* C **468** 2351–5
[30] Nii M, Amemiya N and Nakamura T 2012 Three-dimensional model for numerical electromagnetic field analyses of coated superconductors and its application to Roebel cables *Supercond. Sci. Technol.* **25** 095011
[31] Amemiya N, Miyamoto K, Banno N and Tsukamoto O 1997 Numerical analysis of AC losses in high-Tc superconductors based on E–J characteristics represented with n-value *IEEE Trans. Appl. Supercond.* **7** 2110–3
[32] Amemiya N, Murasawa S, Banno N and Miyamoto K 1998 Numerical modelings of superconducting wires for AC loss calculations *Physica* C **310** 16–29
[33] Kim Y, Hempstead C and Strnad A 1962 Critical persistent currents in hard superconductors *Phys. Rev. Lett.* **9** 306–9
[34] Mifune T, Tominaga N, Sogabe Y, Mizobata Y, Yasunaga M, Ida A, Iwashita T and Amemiya N 2019 Large-scale electromagnetic field analyses of coils wound with coated conductors using a current-vector-potential formulation with a thin-strip approximation *Supercond. Sci. Technol.* **32** 094002
[35] Li Y, Tominaga N, Sogabe Y, Kikuchi T, Wimbush S, Granville S and Amemiya N 2018 Influence of *E–J* characteristics of coated conductors and field ramp-up rates on shielding-current-induced fields of magnet *IEEE Trans. Appl. Supercond.* **28** 4601105
[36] Bonura M and Senatore C 2015 High-field thermal transport properties of REBCO coated conductors *Supercond. Sci. Technol.* **28** 025001
[37] Manfreda G 2011 Review of ROXIE's material properties database for quench simulations *CERN Internal Note* 2011-24 EDMS Nr:1178007